Generation of arbitrary probability distributions from chaotic dynamics

M. J. Poulos ⬤*

Princeton Plasma Physics Laboratory, 100 Stellarator Road, Princeton, New Jersey 08540, USA

A framework is developed to derive nonlinear dynamical systems that chaotically generate arbitrary multivariate probability distributions with smooth, deterministic trajectories. The ideas are used to extend the Nosé-Hoover thermostat methodology to three-dimensional cases where the momentum distribution is nonisotropic and/or non-Gaussian. Toy models that generate several well-known distributions in physics are given as pedagogical examples.

I. INTRODUCTION

The dynamical generation of statistics from trajectories dates back to the seminal work of Langevin (1908) that developed a model of Brownian motion based on the concept of a particle experiencing constant drag and accelerating due to the influence of a stochastic fluctuating force [1]. Choosing the temporal statistics of the force to be Gaussian with vanishing time correlation lead Langevin to trajectory solutions exhibiting the thermal properties of Brownian motion. In the decade following Langevin's work, it was established generally by Fokker and Planck that the ensemble evolution in phase space corresponding with stochastic forcing is modeled by a second-order differential operator [2,3]. The advent of computers further expanded the scope of these efforts with the introduction of the Monte Carlo method, which allowed stochastic processes to be numerically simulated via pseudorandom draws from arbitrary probability distributions. Stochastic models of the Langevin type and their corresponding Fokker-Planck equations have since laid the foundation for a large majority of modern statistical dynamics, providing an explicit means to calculate general ensemble properties for a given stochastic model.

More than 75 years after Langevin's discovery, Nosé (1984) showed for the first time that classical thermodynamic ensembles can also be generated with smooth, deterministic trajectories [4,5]. To do this, Nosé augmented Newtonian mechanics by introducing additional variables to control the fluctuations of kinetic energy such that, in the ergodic limit, the canonical distribution is produced by fluctuations arising from chaotic dynamics. Hoover, using the continuity equation in phase space, refined the approach and identified the essential elements of the dynamical system [6]; the Nosé-Hoover (NH) deterministic thermostat equations have since facilitated a revolution in dynamical simulations, providing novel connections between statistical mechanics and nonlinear dynamics.

In contrast with the Langevin model that has ergodicity built into the stochastic nature of the forcing, the NH thermostat equations are entirely deterministic having phase space ensembles whose evolution is described by first-order differential equations. For this reason, the realization of ergodicity in deterministic models requires the dynamics to be sufficiently chaotic to provide the necessary mixing. Noting the lack of ergodicity in low-dimensional NH models, Martyna, Klein, and Tuckerman (MKT) suggested the use of additional, chained thermostat variables to provide the essential mixing for cases where the original NH dynamics fail to be ergodic [7]. The resulting chained dynamical systems provide one of many routes to achieve ergodicity for a single dynamical trajectory in the reduced phase space.

More recently, it has been shown by Morales that a "chaotic thermostat" may be obtained in a low-dimensional phase space by including an additional sinusoidal forcing term with a phase that self-consistently evolves with the dynamical system [8]. The resulting chaotic system exhibits many similar features to the Langevin model, including diffusion and mobility coefficients that satisfy the Einstein relation. These ideas have been further extended to reduced phase spaces with two dimensions [9], allowing for the ergodic generation of uncorrelated, two-dimensional Gaussian statistics.

While the NH thermostat and the many useful generalizations thereof [8–12] allow Maxwell-Boltzmann statistics to be generated from deterministic dynamics, a natural question arises as to whether these ideas extend to other types of statistics. In this paper, a general approach is introduced to allow arbitrary multivariate probability distributions to be simulated from the smooth chaotic trajectory solutions of deterministic, nonlinear dynamical systems.

The organization of this paper is as follows: Sec. II outlines the generalized framework and elucidates the connection with NH dynamics. Section III uses the generalized framework to derive a general nonlinear dynamical system for the ergodic generation of arbitrary three-dimensional distributions. Three-dimensional isotropization and anisotropization of the trajectory distribution is incorporated within the framework, allowing both the thermal and nonthermal statistics of three-dimensional systems to be modeled within the context of

─────────
*poulos@princeton.edu

chaotic dynamical systems. Specific well-known distributions in physics are studied as pedagogical examples. Conclusions are given in Sec. IV.

II. FORMULATION

Given a dynamical system defined by a flow field in d-dimensional phase space $\dot{z}_\mu = \dot{z}_\mu(z)$, the local conservation of probability requires that the time-dependent distribution function $f = f(t, z)$ be a solution to the continuity equation

$$\frac{\partial f}{\partial t} + \frac{\partial}{\partial z_\mu}(f\dot{z}_\mu) = 0, \tag{1}$$

where summation over repeated indices is assumed unless indicated otherwise. Note that all variables appearing throughout this section are assumed to be dimensionless.

The steady-state distribution $f_0 = f_0(z)$ associated with the dynamical system is a solution to the equation

$$\frac{\partial}{\partial z_\mu}(f_0\dot{z}_\mu) = 0. \tag{2}$$

An ensemble of particles initially distributed according to f_0 will remain so at all later times.

The notion of an ergodic hypothesis relevant here is the assumption that the normalized "histogram" of a single trajectory produced by a dynamical system approaches its associated steady-state distribution, provided the dynamics are sufficiently chaotic to exhibit the necessary mixing in phase space. With $Z_\mu(t)$ a solution of the dynamical system, the ergodic property is expressed as

$$f_0(z) = \lim_{\tau \to \infty} \frac{1}{\tau} \int_0^\tau dt \; \delta^d[z_\mu - Z_\mu(t)], \tag{3}$$

yielding an equivalence between spatial averages over the steady-state distribution and temporal averages over a dynamical trajectory

$$\int d^d z \; f_0(z)\varphi(z) = \lim_{\tau \to \infty} \frac{1}{\tau} \int_0^\tau dt \; \varphi[Z(t)]. \tag{4}$$

Here $\varphi(z)$ is an arbitrary test function on d-dimensional phase space.

Equation (3) is understood as the infinitesimal limit of a discrete-time histogram and is approximated numerically by binning the components of a discrete-time representation of $Z(t)$ on a coarse-grained phase space and normalizing the sum over all bins to unity.

For ergodic dynamics, Eq. (3) provides the direct means to obtain the steady-state distribution given a specified dynamical system. In the complementary situation where it is the steady-state distribution that is specified, a question arises as to how to construct dynamical systems with trajectory solutions that ergodically map to f_0. Progress towards an answer is obtained by considering dynamical systems of the general form

$$\dot{z}_\nu = \frac{1}{f_0} \frac{\partial}{\partial z_\mu}(f_0 S_{\mu\nu}), \tag{5}$$

where $S_{\mu\nu} = S_{\mu\nu}(z)$ is an antisymmetric matrix. It is readily verified that the vanishing divergence requirement of Eq. (2)

is automatically satisfied for any choice of f_0:

$$\frac{\partial}{\partial z_\nu}(f_0\dot{z}_\nu) = \frac{\partial}{\partial z_\mu}\frac{\partial}{\partial z_\nu}(f_0 S_{\mu\nu}) = 0. \tag{6}$$

Thus, if $S_{\mu\nu}$ is chosen such that the resulting dynamical system exhibits ergodicity, then the trajectories generated by Eq. (5) will have histograms that tend to the steady-state distribution f_0.

Equation (5) corresponds to a general class of dynamics that encompass both Hamiltonian mechanics and Nosé-Hoover dynamics, as will be shown next in this section. In Sec. III it is shown with examples how specific choices of $S_{\mu\nu}$ easily lead to well-behaved chaotic dynamical systems exhibiting the desired ergodic statistics determined by the arbitrary choice of f_0.

Nosé-Hoover dynamics

To examine features and implications of Eq. (5), a set of examples are considered. First note that any Hamiltonian system admits a representation in the form of Eq. (5). For a $2n$-dimensional phase space with $\mathbf{x} \equiv \{z_1, \ldots, z_n\}$ and $\mathbf{p} \equiv \{z_{n+1}, \ldots, z_{2n}\}$, the choices in Eq. (5) of antisymmetric matrix

$$S_{\mu\nu} = T \begin{bmatrix} 0 & I_n \\ -I_n & 0 \end{bmatrix} \tag{7}$$

and steady-state distribution

$$f_0 \sim e^{-H/T} \tag{8}$$

lead directly to Hamilton's equation of motion. Here I_n is the n-dimensional identity matrix.

The Nosé-Hoover augmented system in $(2n + 1)$-dimensional phase space also admits a representation in the form of Eq. (5). The choices of antisymmetric matrix

$$S_{\mu\nu} = T \begin{bmatrix} 0 & I_n & 0 \\ -I_n & 0 & -\mathbf{p}/Q \\ 0 & \mathbf{p}^T/Q & 0 \end{bmatrix} \tag{9}$$

and steady-state distribution

$$f_0 \sim e^{-(H+Q\zeta^2/2)/T} \tag{10}$$

yield the Nosé-Hoover thermostat equations

$$\dot{\mathbf{x}} = \frac{\partial H}{\partial \mathbf{p}}, \tag{11}$$

$$\dot{\mathbf{p}} = -\frac{\partial H}{\partial \mathbf{x}} - \zeta \mathbf{p}, \tag{12}$$

$$\dot{\zeta} = \frac{1}{Q}\left(\mathbf{p} \cdot \frac{\partial H}{\partial \mathbf{p}} - nT\right), \tag{13}$$

where $\zeta \equiv z_{2n+1}$ is an additional control variable.

Note that the dependence of $S_{\mu\nu}$ on the phase space variables is closely linked with presence of a nonzero Lyapunov spectrum, as

$$\frac{\partial}{\partial z_\nu}\dot{z}_\nu = \frac{\partial \ln f_0}{\partial z_\mu}\frac{\partial S_{\mu\nu}}{\partial z_\nu}. \tag{14}$$

While originally formulated for Hamiltonian dynamics in molecular simulations, the insights gained from the NH thermostat are viewed here in a more general context of nonlinear

control theory. For a set of k variables $\{z_1, z_2, \ldots, z_k\}$ that fluctuate in accord with a set of arbitrary forcing functions,

$$\dot{z}_\nu = F_\nu(t), \tag{15}$$

the question is how to dynamically control the fluctuations of z_ν via additional self-consistent forcing such that certain statistical requirements are met. To do this, an enlarged phase space is introduced with additional control variables $\{z_{k+1}, \ldots, z_n\}$ that couple to the first k variables in the form of Eq. (5). A point in the extended phase space satisfies

$$\dot{z}_\nu = F_\nu(t) + \frac{1}{f_0} \frac{\partial}{\partial z_\mu} (f_0 S_{\mu\nu}). \tag{16}$$

For a two-dimensional phase space with variables $\{z_1, z_2\}$, Eq. (16) leads to

$$\dot{z}_1 = F(t) - \frac{1}{f_0} \frac{\partial}{\partial z_2} (f_0 S_{12}), \tag{17}$$

$$\dot{z}_2 = \frac{1}{f_0} \frac{\partial}{\partial z_1} (f_0 S_{12}). \tag{18}$$

Choosing f_0 to be the product of individual Gaussians and S_{12} to be proportional to $-z_1$, leads to the simplest realization of the forced NH thermostat. This two-dimensional forced system has been the subject of several detailed studies that are worth mentioning here. In Ref. [13], the effect of sinusoidal forcing was analyzed in detail, where it was found that nontrivial features arise as the phase and amplitude of the applied force are varied. It was also shown in Ref. [8] that the phase of the sinusoidal force can be self-consistently driven by the second variable to produce a chaotic system in three-dimensional phase space. While these studies explored the generic case corresponding to Gaussian statistics, the general formulation presented here suggests that more exotic statics may be studied within a similar deterministic framework.

In the absence of forcing, it is important to note that two-dimensional systems are never ergodic and low-dimensional systems will often fail to be ergodic, and so, to obtain the requisite mixing in phase space, additional degrees of freedom should be included in the dynamics.

One route to this inclusion is with the particular choice

$$S_{\mu\nu} = z_\nu \delta_{\mu, \nu+1} - z_\mu \delta_{\nu, \mu+1}, \tag{19}$$

leading to the "chained" dynamical system

$$\dot{z}_\nu = \frac{1}{f_0} \left[\frac{\partial}{\partial z_{\nu+1}} (z_\nu f_0) - \frac{\partial}{\partial z_{\nu-1}} (z_{\nu-1} f_0) \right], \tag{20}$$

where no summation over the repeated indices is assumed.

For the specific case with f_0 given by the product of individual Gaussians, Eq. (20) produces the MKT chain dynamics [7].

III. THREE-DIMENSIONAL FLUCTUATION CONTROL

The case studied in this section is obtained in seven-dimensional phase space with the choice

$$S_{\mu\nu} = \begin{bmatrix} 0 & [\mathbf{p}]_\times & -\mathbf{p} \\ [\mathbf{p}]_\times & 0 & -\zeta(\mathbf{\Gamma} - \mathbf{p}) \\ \mathbf{p}^T & \zeta(\mathbf{\Gamma} - \mathbf{p})^T & 0 \end{bmatrix}, \tag{21}$$

where the three-dimensional vectors are $\mathbf{p} \equiv \{z_1, z_2, z_3\}$ and $\mathbf{\Gamma} \equiv \{z_4, z_5, z_6\}$, and the scalar is $\zeta \equiv z_7$. The three-dimensional matrix $[\mathbf{p}]_\times$ denotes the cross product matrix of $\mathbf{p}$.

Taking the steady-state distribution to be

$$f_0 \sim f_\mathbf{p}(\mathbf{p}) e^{-\Gamma^2/2 - \zeta^2/2}, \tag{22}$$

where $\Gamma^2 \equiv \mathbf{\Gamma} \cdot \mathbf{\Gamma}$, and defining the auxiliary vector $\mathbf{L_p}$ as

$$\mathbf{L_p} \equiv -\frac{\partial \ln f_\mathbf{p}}{\partial \mathbf{p}}, \tag{23}$$

the dynamical system derived from Eqs. (5) and (21) takes the form

$$\dot{\mathbf{p}} = \mathbf{\Gamma} \times \mathbf{p} - \zeta \mathbf{p}, \tag{24}$$

$$\dot{\mathbf{\Gamma}} = \mathbf{L_p} \times \mathbf{p} - (\zeta^2 - 1)(\mathbf{\Gamma} - \mathbf{p}), \tag{25}$$

$$\dot{\zeta} = \mathbf{L_p} \cdot \mathbf{p} - 3 + \zeta[\mathbf{\Gamma} \cdot (\mathbf{\Gamma} - \mathbf{p}) - 3]. \tag{26}$$

Equations (24)–(26) have an interpretation as a chaotic, deterministic Langevin model, where the vector $\mathbf{p}$ is a three-dimensional momentum. The scalar ζ controls the length of $\mathbf{p}$ and the vector $\mathbf{\Gamma}$ controls rotations of $\mathbf{p}$. The coupling between $\mathbf{\Gamma}$ and ζ generates the mixing necessary for ergodicity. Note that for any isotropic $f_\mathbf{p}$, the first term on the r.h.s. of Eq. (25) vanishes.

A. Isotropic statistics

1. Isotropic Nosé-Hoover thermostat

For isotropic Gaussian statistics, $f_\mathbf{p}$ is given by

$$f_\mathbf{p} \sim e^{-\beta p^2/2}, \tag{27}$$

where $p^2 \equiv \mathbf{p} \cdot \mathbf{p}$. The auxiliary vector [Eq. (23)] is linear in the momentum

$$\mathbf{L_p} = \beta \mathbf{p}, \tag{28}$$

and the dynamical system given by Eqs. (24)–(26) is

$$\dot{\mathbf{p}} = \mathbf{\Gamma} \times \mathbf{p} - \zeta \mathbf{p}, \tag{29}$$

$$\dot{\mathbf{\Gamma}} = -(\zeta^2 - 1)(\mathbf{\Gamma} - \mathbf{p}), \tag{30}$$

$$\dot{\zeta} = \beta p^2 - 3 + \zeta[\mathbf{\Gamma} \cdot (\mathbf{\Gamma} - \mathbf{p}) - 3]. \tag{31}$$

With initial nonzero values of $\mathbf{p}$ and $\mathbf{\Gamma}$ pointing in different directions, a single dynamical trajectory in seven-dimensional phase space ergodically generates uncorrelated, three-dimensional Gaussian statistics for $\mathbf{p}$.

Figure 1 shows three snapshots of a single dynamical trajectory obtained by numerically solving Eqs. (29)–(31). The numerical integration is carried out using a fourth-order Runge-Kutta scheme with a time step equal to $dt = 0.01$. The initial conditions used are $\mathbf{p}_0 = (0.5, 0, 0)$, $\mathbf{\Gamma}_0 = (0, 0.5, 0)$, and $\zeta_0 = 0$. The inverse temperature is taken to be $\beta = 1$.

Figure 2 shows the time-series histograms (dashed red curves) in the time interval $t \in \{0, 20\,000\}$ for each component of $\mathbf{p}$ generated with Eqs. (29)–(31). The black solid
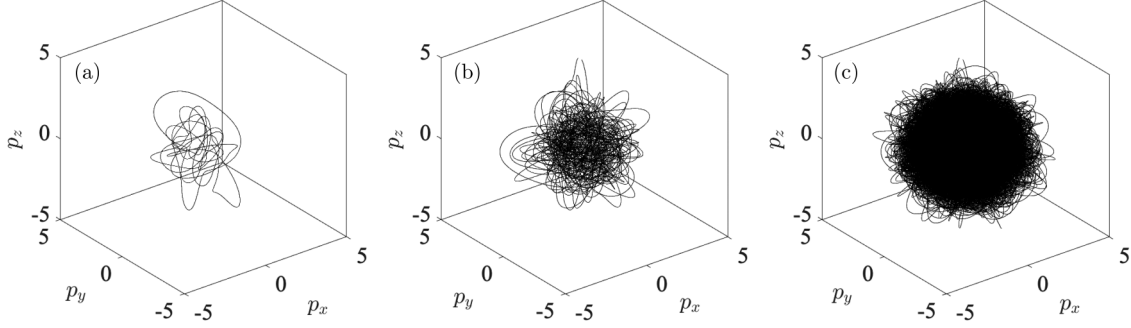
FIG. 1. A single trajectory from the isotropic three-dimensional thermostat (Gaussian distribution) obtained by numerically solving Eqs. (29)–(31). The initial conditions at $t = 0$ are $\mathbf{p}_0 = (0.5, 0, 0)$, $\mathbf{\Gamma}_0 = (0, 0.5, 0)$, and $\zeta_0 = 0$. Panels (a), (b), and (c) show the history of the trajectory for times t less than 50, 500, and 20 000, respectively. The inverse temperature is $\beta = 1$, and the time step used in the fourth-order Runge-Kutta scheme is equal to $dt = 0.01$

curves indicate the analytic steady-state Gaussian distributions. From the figure it is evident that each histogram very closely approximates a Gaussian distribution.

It is further verified numerically that the covariance matrix of $\mathbf{p}$ tends to identity

$$\frac{1}{\tau} \int_0^\tau dt \, \mathbf{p}(t)\mathbf{p}(t) \to \frac{1}{\beta} \mathbf{I}_3, \tag{32}$$

as to be expected for uncorrelated, three-dimensional Gaussian statistics.

2. Isotropic Planck distribution: A thermostat for the noninteracting photon gas

The general framework considered here allows the notion of a thermostat to be extended to cases where the steady-state distribution is non-Gaussian. For pedagogical purposes, the general case of thermal equilibrium is considered. The momentum distribution has the form

$$f_{\mathbf{p}} \sim \frac{1}{e^{\beta[H(\mathbf{p})-\mu]} - \xi}, \tag{33}$$

where β is the inverse temperature, μ is the chemical potential, and ξ is the statistical sign. Fermi-Dirac statistics correspond to $\xi = -1$, Maxwell-Boltzmann statistics to $\xi = 0$, and Bose-Einstein statistics to $\xi = 1$.

The Planck distribution ($H = p$, $\mu = 0$, $\xi = 1$) has the form

$$f_{\mathbf{p}} \sim \frac{1}{e^{\beta p} - 1}, \tag{34}$$

where $p \equiv \sqrt{\mathbf{p} \cdot \mathbf{p}}$. The logarithmic derivative leads to the auxiliary vector [Eq. (23)]

$$\mathbf{L_p} = \frac{\beta \hat{\mathbf{p}}}{1 - e^{-\beta p}}, \tag{35}$$

and the dynamical system derived from Eqs. (24)–(26) is

$$\dot{\mathbf{p}} = \mathbf{\Gamma} \times \mathbf{p} - \zeta \mathbf{p}, \tag{36}$$

$$\dot{\mathbf{\Gamma}} = -(\zeta^2 - 1)(\mathbf{\Gamma} - \mathbf{p}), \tag{37}$$

$$\dot{\zeta} = \frac{\beta p}{1 - e^{-\beta p}} - 3 + \zeta[\mathbf{\Gamma} \cdot (\mathbf{\Gamma} - \mathbf{p}) - 3]. \tag{38}$$

Equations (36)–(38) produce from a single dynamical trajectory time-averaged statistics corresponding to the Planck distribution. Furthermore, as a consequence of the ergodic nature of the dynamics, an ensemble of seven-dimensional points that each separately evolve according to Eqs. (36)–(38) will yield ensemble statistics that tend to the Planck distribution in the long-time limit.

Three snapshots of a single dynamical trajectory obtained from the numerical solution of Eqs. (36)–(38) are shown
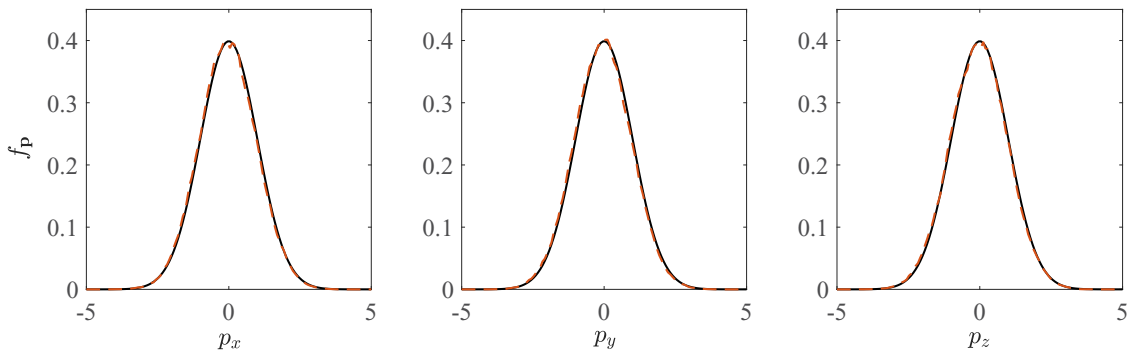
FIG. 2. Normalized histograms in the time interval $t \in \{0, 20\,000\}$ for each component of the momentum obtained from a single trajectory solution of Eqs. (29)–(31) (dashed red curves). The solid black curves indicate projections of the analytic steady-state Gaussian distribution. From the figure, it is evident that the distributions for each component are closely approximated by Gaussian distributions.
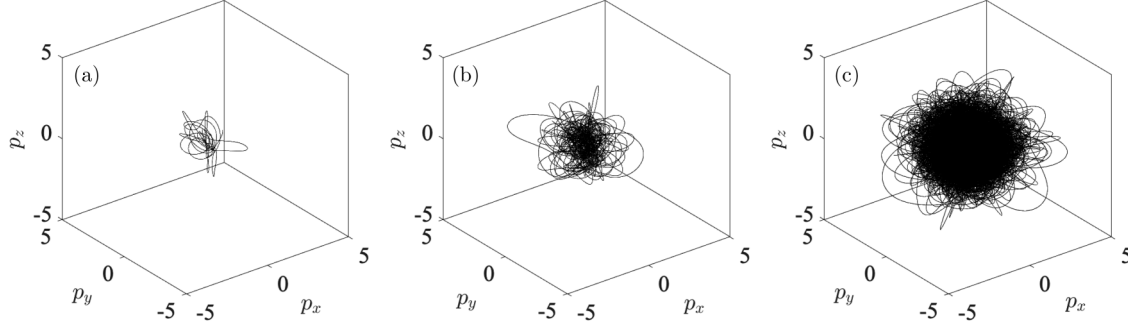
FIG. 3. A single trajectory generated by the thermostat for the photon gas (Planck distribution) obtained by numerically solving Eqs. (36)–(38). The initial conditions are $\mathbf{p}_0 = (0.5, 0, 0)$, $\boldsymbol{\Gamma}_0 = (0, 0.5, 0)$, and $\zeta_0 = 0$, the inverse temperature is $\beta = 3$. Panels (a), (b), and (c) show the history of the trajectory for times t less than 50, 500, and 20 000, respectively.

in Fig. 3. The initial conditions are $\mathbf{p}_0 = (0.5, 0, 0)$, $\boldsymbol{\Gamma}_0 = (0, 0.5, 0)$, and $\zeta_0 = 0$; the inverse temperature is $\beta = 3$. The time integration is performed for $t \in \{0, 20\,000\}$ using a fourth-order Runge-Kutta scheme with a time step $dt = 0.01$.

The number of intersections of a three-dimensional trajectory $\mathbf{p}(t)$ with a shell in momentum-space corresponding to energy E is

$$f_E = \lim_{\tau \to \infty} \frac{1}{\tau} \int_0^\tau dt \, \delta\{E - H[\mathbf{p}(t)]\}, \tag{39}$$

and the corresponding distribution of energy is the product $U_E \equiv E f_E$, or

$$U_E = \lim_{\tau \to \infty} \frac{E}{\tau} \int_0^\tau dt \, \delta\{E - H[\mathbf{p}(t)]\}. \tag{40}$$

Analytically, the Jacobian due to the change of variables

$$f_{\mathbf{p}} d^3 p \sim f_{\mathbf{p}} p^2 dp \sim f_E dE \tag{41}$$

yields the proportionality between f_E and $f_{\mathbf{p}}$:

$$f_E \sim p^2 \left| \frac{dp}{dE} \right| f_{\mathbf{p}}. \tag{42}$$

For the Planck distribution, the distribution of energy is

$$U_E \sim \frac{E^3}{e^{\beta E} - 1}. \tag{43}$$

Figure 4 compares the numerically calculated distribution of energy from Eq. (40) (dashed red curve) with the analytic expectation from Eq. (43) (solid black curve). The trajectory $\mathbf{p}(t)$ corresponds to the numerical solution of Eqs. (36)–(38), with the same parameters used in Fig. 3. From the figure, it is clear that the time-averaged statistics of a single trajectory are closely representative of the Planck distribution.

3. Isotropic Fermi distribution: A thermostat for the noninteracting free-electron gas

The Fermi distribution ($H = p^2/2$, $\mu = E_F$, $\xi = -1$) has the form

$$f_{\mathbf{p}} \sim \frac{1}{e^{\beta(p^2/2 - E_F)} + 1}, \tag{44}$$

which leads to the auxiliary vector [Eq. (23)]

$$\mathbf{L_p} = \frac{\beta \mathbf{p}}{1 + e^{-\beta(p^2/2 - E_F)}}. \tag{45}$$

The dynamical system derived from Eqs. (24)–(26) is then

$$\dot{\mathbf{p}} = \boldsymbol{\Gamma} \times \mathbf{p} - \zeta \mathbf{p}, \tag{46}$$

$$\dot{\boldsymbol{\Gamma}} = -(\zeta^2 - 1)(\boldsymbol{\Gamma} - \mathbf{p}), \tag{47}$$

$$\dot{\zeta} = \frac{\beta p^2}{1 + e^{-\beta(p^2/2 - E_F)}} - 3 + \zeta[\boldsymbol{\Gamma} \cdot (\boldsymbol{\Gamma} - \mathbf{p}) - 3]. \tag{48}$$

Figure 5 shows three snapshots of a single trajectory obtained by numerically solving Eqs. (46)–(48). Figures 5(a)–5(c) show the history of the trajectory for times less than 100, 500, and 20 000, respectively. The initial conditions are $\mathbf{p}_0 = (0.5, 0, 0)$, $\boldsymbol{\Gamma}_0 = (0, 0.5, 0)$, $\zeta_0 = 0$, the inverse temperature is $\beta = 2$, and the Fermi energy is $E_f = 4$. The time integration is performed using a fourth-order Runge-Kutta technique in the interval $t \in \{0, 20\,000\}$, with a time step equal to $dt = 0.01$.
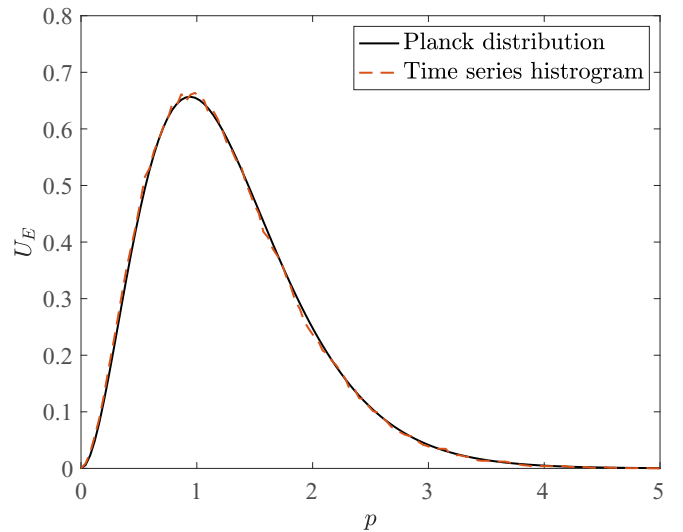
FIG. 4. Normalized energy histogram of a single dynamical trajectory obtained by numerically solving Eqs. (36)–(38). The red dashed curve corresponds to the numerically computed energy histogram, and the solid black curve is the analytic expression for the Planck distribution. The inverse temperature is $\beta = 3$.
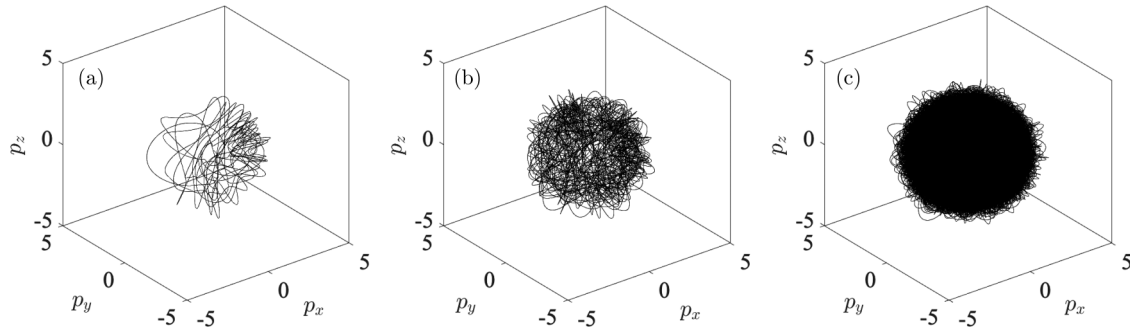
FIG. 5. A single trajectory generated by the thermostat for the free-electron gas (Fermi distribution) obtained by numerically solving Eqs. (46)–(48). The initial conditions are $\mathbf{p}_0 = (0.5, 0, 0)$, $\mathbf{\Gamma}_0 = (0, 0.5, 0)$, $\zeta_0 = 0$, the inverse temperature is $\beta = 2$, and the Fermi energy is $E_f = 4$. Panels (a), (b), and (c) show the history of the trajectory for times less than 100, 500, and 20 000, respectively.

The analytic distribution of energy for the Fermi distribution is proportional to

$$U_E \sim \frac{E^{3/2}}{e^{\beta(E-E_F)} + 1},\tag{49}$$

and the numerical distribution is obtained from Eq. (40).

Figure 6 compares the numerically calculated distribution of energy from Eq. (40) with trajectory $\mathbf{p}(t)$ corresponding to the numerical solution of Eqs. (46)–(48) (dashed red curve) with the analytic expectation from Eq. (49) (solid black curve). The parameters are the same as those used in Fig. 5. From the figure, it is evident that the time-averaged statistics of the chaotic trajectory are closely representative of the Fermi distribution.

Similar to the previous cases studied, Eqs. (46)–(48) have two interpretations. The first interpretation considers populating the point in momentum space $\mathbf{p}(t)$ during the time-interval $[t, t + dt]$. For evenly spaced intervals in time, the resulting distribution generated will tend to the Fermi distribution. The second interpretation considers an ensemble of seven-dimensional phase space points that occupy a nonzero volume. Under the prescribed evolution, the ensemble will tend to the Fermi distribution. As in the previous cases, the connection between these two interpretations is a result of ergodicity.

4. Exponential frequency spectra

One identifying characteristic of chaotic dynamics is the exponential dependence of frequency spectra for large frequencies. As noted in Ref. [14], this exponential dependence can be related to the analytic continuation of the dynamical system to complex time. The contour defining the Fourier transform integration may be deformed into the upper half of the complex plane, where it attains a contribution from the first pole closest to the real axis. This feature has been used previously to identify chaotic dynamics present in laboratory environments (e.g., in magnetized plasmas [15]).

Figure 7 displays in semilog format the frequency spectra corresponding to the momentum magnitudes for each of the three thermostat models considered previously. For large frequencies, the exponential dependence characteristic of chaotic
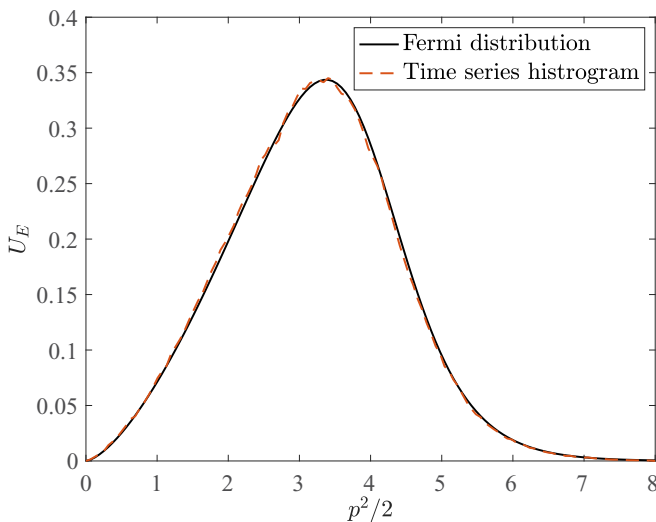
FIG. 6. Normalized energy histogram of a single dynamical trajectory obtained by numerically solving Eqs. (46)–(48). The inverse temperature is $\beta = 3$, and the Fermi energy is $E_F = 5$.
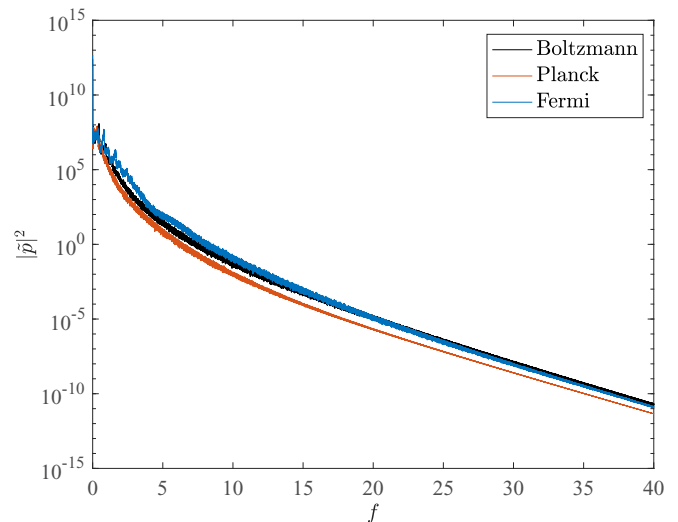
FIG. 7. Semilog display of the frequency spectra corresponding to the momentum magnitudes for each of the isotropic thermostats. The exponential dependence of the spectra for large frequencies is characteristic of chaotic dynamics.

dynamics is present. Notably, the exponential decay constants for each of the three systems are nearly identical, which can be partially attributed to the similarities of the Lyapunov spectra for each of the three systems [14].

B. Anisotropic statistics

1. Multivariate Gaussian distributions: An anisotropic thermostat for pressure tensor control

Equations (24)–(26) allow for anisotropy in the steady-state distribution. One of the simplest cases is the multivariate Gaussian distribution

$$f_{\mathbf{p}} \sim e^{-\frac{1}{2}\mathbf{p}\cdot\mathbf{\Sigma}_p^{-1}\cdot\mathbf{p}}, \tag{50}$$

where $\mathbf{\Sigma}_p$ is the symmetric 3×3 covariance matrix of $\mathbf{p}$. The auxiliary vector is

$$\mathbf{L_p} = \mathbf{\Sigma}_p^{-1} \cdot \mathbf{p}, \tag{51}$$

and the dynamical system given by Eqs. (24)–(26) takes the form

$$\dot{\mathbf{p}} = \mathbf{\Gamma} \times \mathbf{p} - \zeta\mathbf{p}, \tag{52}$$

$$\dot{\mathbf{\Gamma}} = \left(\mathbf{\Sigma}_p^{-1} \cdot \mathbf{p}\right) \times \mathbf{p} - (\zeta^2 - 1)(\mathbf{\Gamma} - \mathbf{p}), \tag{53}$$

$$\dot{\zeta} = \mathbf{p} \cdot \mathbf{\Sigma}_p^{-1} \cdot \mathbf{p} - 3 + \zeta[\mathbf{\Gamma} \cdot (\mathbf{\Gamma} - \mathbf{p}) - 3]. \tag{54}$$

Each component of $\mathbf{p}$ has a histogram that tends toward a Gaussian distribution. However, there are now nonvanishing correlations between different components of $\mathbf{p}$ determined by the off-diagonal elements of $\mathbf{\Sigma}_p$:

$$\frac{1}{\tau} \int_0^\tau dt \; \mathbf{p}(t)\mathbf{p}(t) \to \mathbf{\Sigma}_p. \tag{55}$$

A single particle evolving in accord with Eqs. (53)–(54) will chaotically generate time-averaged statistics that tend to the specified multivariate Gaussian distribution. Furthermore, due to the ergodic nature of the dynamics, an ensemble of particles occupying a nonzero phase volume that each separately evolve according to Eqs. (53)–(54) will produce ensemble statistics that also tend to the specified multivariate Gaussian distribution.

2. Extreme anisotropy: "CHAOS" distribution

The distribution function used in Eqs. (24)–(26) is not limited to have a specific shape, size, or symmetry; it can be arbitrarily chosen with the minor caveat that it should consist of topologically connected regions. If a region in phase space with zero measure completely separates two or more nonzero-measure "lobes," the dynamics will stay confined to only one of the lobes.

As a final example to illustrate the versatility of Eqs. (24)–(26), a distribution function that spells out the word "CHAOS" is chosen. The distribution is essentially composed of five neighboring "figure-8" distributions with certain edges selectively removed. There is small overlap between the different letters of the word so that the entire distribution is one topologically connected three-dimensional region in the reduced phase space. An analytic form for the distribution (given in
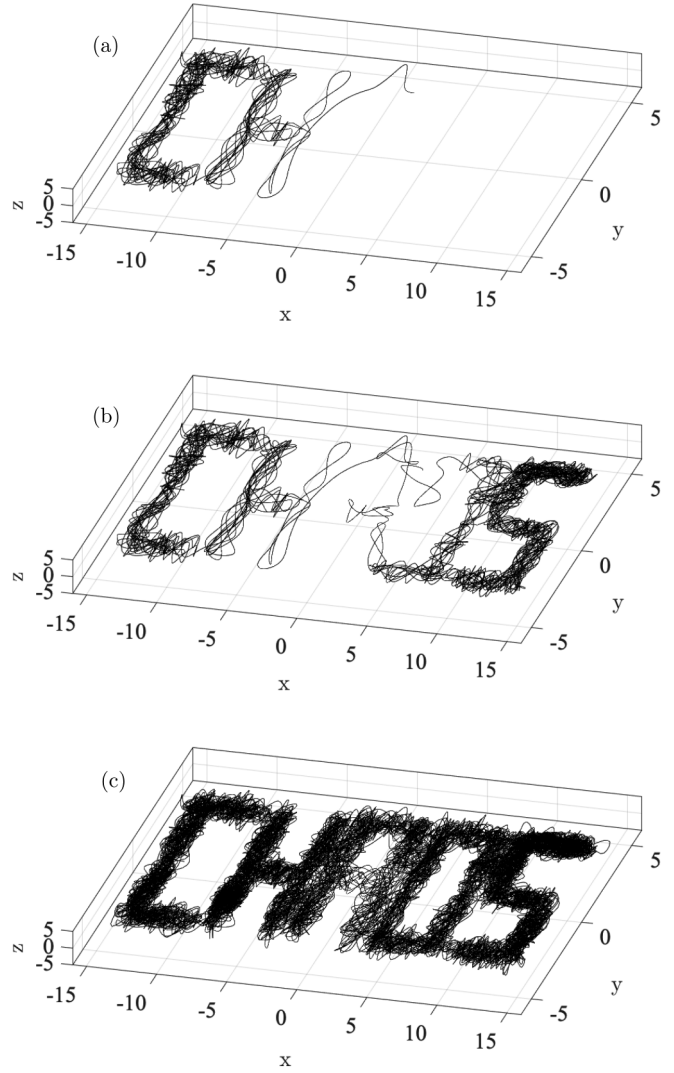
FIG. 8. A single dynamical trajectory produced by Eqs. (24)–(26). Panels (a), (b), and (c) show the history of the trajectory for times less than 50, 150, and 1000, respectively.

the Appendix) is used to evaluate the auxiliary vector $\mathbf{L_p}$ in Eqs. (24)–(26), leading to a seven-dimensional chaotic dynamical system.

Figure 8 shows the history of a single dynamical trajectory produced using this exotic distribution. The time integration is performed with a fourth-order Runge-Kutta scheme with time step equal to 0.01. The initial conditions are $\mathbf{p}_0 = (-12.2, 0, 0)$, $\mathbf{\Gamma}_0 = (0, 0.5, 0)$, and $\zeta_0 = 0$. Figures 8(a)–8(c) show the history of the trajectory for times less than 50, 150, and 1000, respectively. For times greater than 1000, the word "CHAOS" is clearly visible.

While there is clearly not a physical situation described by such a distribution, considerations of this variety show the extremes for malleability and controllability of low-dimensional chaotic systems. The ability to generate an extremely asymmetric distribution, such as a word, indicates the generality of the underlying equations and the ease with which other distributions may be reliably generated.

IV. CONCLUSIONS

In this paper, a framework was developed to derive nonlinear dynamical systems that chaotically generate arbitrary probability distributions. Using the continuity equation in n-dimensional phase space, a general class of dynamics was identified. Several specific examples of dynamical systems were derived and shown to have the desired specified statistical properties. For isotropic three-dimensional cases, the methodology was used to produce Maxwell-Boltzmann, Bose-Einstein, and Fermi-Dirac statistics. It was also shown with an exotic anisotropic case that the formulation allows arbitrarily shaped distributions to be reliably produced, indicating the generality of the underlying framework.

For the case of three-dimensional statistics, the matrix in Eq. (21) is certainly not unique, and there is likely an infinite class of antisymmetric matrices that also lead naturally to well-behaved chaotic dynamics. A fruitful route for future research is to identify other such antisymmetric matrices and contrast the resulting dynamics.

In the situation where the steady-state distribution is composed of topologically disconnected regions (i.e., two or more nonzero-measure regions completely separated by a region with zero measure), the dynamics given by Eq. (5) will remain localized to only one connected portion of the domain. To continuously generate a probability distribution that is topologically disconnected, a separate trajectory for each connected region must be considered. Alternatively, discontinuous "jumping" from one connected region to another may also allow for dynamic generation of the statistics; however, this nonlocality requires features outside the scope of continuous dynamical systems.

While the examples given in this paper primarily focused on the ergodic generation of noninteracting particle statistics, it should be noted that the addition of a potential in the Hamiltonians considered allows for the incorporation of interactions. An externally imposed potential is straightforward to implement and requires only a small modification to the underlying equations. A self-consistent potential, however, requires a larger modification and can either be handled with an ensemble of trajectories or with a self-consistent time integration performed over an ergodic history. Implementation of a self-consistent potential may permit several new interesting studies.

APPENDIX: CHAOS DISTRIBUTION

Here the analytic form of the exotic distribution function used in Sec. III B 2 is given. For ease of notation, let $\{p_x, p_y, p_z\} \rightarrow \{x, y, z\}$. One edge of a single letter is de-

scribed by the (non-normalized) distribution function

$$f_e(x, y, z; \beta_x, \beta_y, \beta_z, \alpha) = \frac{e^{-\beta_z z^2}}{1 + e^{\beta_x x^2 + \beta_y y^2 - \alpha}}. \qquad (A1)$$

Defining the arrays

$$x_i = \{0, 0, 0, -2, 2, -2, 2\}, \qquad (A2)$$

$$y_i = \{3.5, 0, -3.5, 1.8, 1.8, -1.8, -1.8\}, \qquad (A3)$$

$$\beta_{x,i} = \{0.5, 1, 0.5, 5, 5, 5, 5\}, \qquad (A4)$$

$$\beta_{y,i} = \{10, 10, 10, 1, 1, 1, 1\}, \qquad (A5)$$

and the global constants

$$\beta_z = 1/2, \quad \alpha = 3, \qquad (A6)$$

the distribution for a single letter can be written as a sum over seven edges:

$$F_L(x, y, z; \{\xi_i\}) = \sum_{i=1}^{7} \xi_i f_e(x - x_i, y - y_i, z; \beta_{x,i}, \beta_{y,i}, \beta_z, \alpha). \qquad (A7)$$

The seven bits $\xi_i \in \{0, 1\}$ for $i \in \{1, \ldots, 7\}$, determine which edges are active and which are removed. For $\xi_i = \{1, 1, 1, 1, 1, 1, 1\}$ (i.e., all edges active), the resulting distribution is a "figure-8." Each of the five letters in the word "CHAOS" can be represented by different choices for the seven bits.

Explicitly, let

$$C: \xi_i^1 = \{1, 0, 1, 1, 0, 1, 0\}, \qquad (A8)$$

$$H: \xi_i^2 = \{0, 1, 0, 1, 1, 1, 1\}, \qquad (A9)$$

$$A: \xi_i^3 = \{1, 1, 0, 1, 1, 1, 1\}, \qquad (A10)$$

$$O: \xi_i^4 = \{1, 0, 1, 1, 1, 1, 1\}, \qquad (A11)$$

$$S: \xi_i^5 = \{1, 1, 1, 1, 0, 0, 1\}. \qquad (A12)$$

With the horizontal shifts

$$h^j = \{-11.5, -5.75, 0, 5.75, 11.5\}, \qquad (A13)$$

the distribution for the word "CHAOS" is given by

$$f_{\text{CHAOS}} \sim \sum_{j=1}^{5} F_L\left(x - h^j, y, z; \left\{\xi_i^j\right\}\right). \qquad (A14)$$

The gradient of this distribution, ∇f_{CHAOS}, is obtained by replacing f_e in Eq. (A7) with its gradient

$$\nabla f_e = -2\beta_z z \hat{\mathbf{z}} f_e - \frac{2(\beta_x x \hat{\mathbf{x}} + \beta_y y \hat{\mathbf{y}})}{1 + e^{-\beta_x x^2 - \beta_y y^2 + \alpha}} f_e. \qquad (A15)$$

The auxiliary vector $\mathbf{L_p}$ is then obtained as

$$\mathbf{L_p} = -\frac{\nabla f_{\text{CHAOS}}}{f_{\text{CHAOS}}}. \qquad (A16)$$

While the vector $\mathbf{L_p}$ is analytically well defined for all $\{x, y, z\}$, care must be taken to ensure that its numerical evaluation remains finite as $f_e \rightarrow 0$.

[1] P. Langevin, Sur la théorie du mouvement brownien [On the theory of Brownian motion], CR Acad. Sci. **146**, 530 (1908).

[2] A. D. Fokker, Die mittlere Energie rotierender elektrischer Dipole im Strahlungsfeld, Ann. Phys. **348**, 810 (1914).

[3] M. Planck, Über einen Satz der statistischen Dynamik und seine Erweiterung in der Quantentheorie, Sitzber. Preuss. Akad. Wissenschaf. Berlin **24**, 324 (1917).

[4] S. Nosé, A unified formulation of the constant temperature molecular dynamics methods, J. Chem. Phys. **81**, 511 (1984).

[5] S. Nosé, A molecular dynamics method for simulations in the canonical ensemble, Mol. Phys. **52**, 255 (1984).

[6] W. G. Hoover, Canonical dynamics: Equilibrium phase-space distributions, Phys. Rev. A **31**, 1695 (1985).

[7] G. J. Martyna, M. L. Klein, and M. Tuckerman, Nosé-Hoover chains: The canonical ensemble via continuous dynamics, J. Chem. Phys. **97**, 2635 (1992).

[8] G. J. Morales, Investigation of a chaotic thermostat, Phys. Rev. E **97**, 032203 (2018).

[9] G. J. Morales, Two-dimensional chaotic thermostat and behavior of a thermalized charge in a weak magnetic field, Phys. Rev. E **99**, 062218 (2019).

[10] A. Bulgac and D. Kusnezov, Deterministic and time-reversal invariant description of Brownian motion, Phys. Lett. A **151**, 122 (1990).

[11] W. G. Hoover, J. C. Sprott, and C. G. Hoover, Ergodicity of a singly-thermostated harmonic oscillator, Commun. Nonlinear Sci. Numer. Simulat. **32**, 234 (2016).

[12] H. Hüffel and S. Ilijić, Ergostatting and thermostatting at a fixed point, Phys. Rev. E **94**, 052115 (2016).

[13] Y. Zhao and G. J. Morales, Properties of a sinusoidally driven thermostat, Phys. Rev. E **98**, 022213 (2018).

[14] D. E. Sigeti, Exponential decay of power spectra at high frequency and positive Lyapunov exponents, Physica D **82**, 136 (1995).

[15] D. C. Pace, M. Shi, J. E. Maggs, G. J. Morales, and T. A. Carter, Exponential frequency spectrum and Lorentzian pulses in magnetized plasmas, Phys. Plasmas **15**, 122304 (2008).